NASA Technical Memorandum 4071

A Water Tunnel Study of Gurney Flaps

Dan H. Neuhart and Odis C. Pendergraft, Jr.

NOVEMBER 1988

NASA

NASA Technical Memorandum 4071

A Water Tunnel Study of Gurney Flaps

Dan H. Neuhart
PRC Systems Services
A Division of Planning Research Corporation
Hampton, Virginia

Odis C. Pendergraft, Jr.
Langley Research Center
Hampton, Virginia

National Aeronautics
and Space Administration

Scientific and Technical
Information Division

1988

Summary

Flow visualization tests of several Gurney flap configurations were made in the Langley 16- by 24-Inch Water Tunnel at a Reynolds number of 8588. Relative to the wing without the flaps, these devices provided an increased region of attached flow on a wing upper surface for angles of attack below 3.5°. The recirculation region behind the flap was visualized and shown to be consistent with hypotheses stated in previous research. Although the test Reynolds number for this study was several orders of magnitude below those in previous investigations, the effect of the Gurney flaps was in qualitative agreement with the investigations. This is as would be expected from first-order effects for high-lift devices.

Introduction

The present study was undertaken to investigate visually the flow field near a Gurney flap and to study the effects of the flap on flow separation on a wing upper surface. Water tunnel observations can provide valuable visual perspective of the flow fields. Although previous researchers have found that larger flaps (i.e., greater than 1.25 percent chord) produce large drag penalties, a set of larger flaps were tested here to provide visual insight into the structure of the flow in the trailing-edge region. A Gurney flap is simply a flat plate located at the airfoil trailing edge perpendicular to the chord line on the pressure side of the airfoil. It is primarily used for increasing lift. As occurs with other trailing-edge high-lift devices, the Gurney flap reduces the angle of attack for zero lift α_o and increases the maximum lift coefficient $C_{L,\max}$, while it slightly increases the lift-curve slope C_{L_α}. The effects of this device on drag, however, are not generally as well defined. Some studies show drag reductions, some show no net drag change, and some show drag increases relative to clean-trailing-edge configurations.

Liebeck (ref. 1) reported on the improved airfoil high-lift characteristics obtained by using the Gurney flap. The effects of Gurney flaps were cited in two examples. One was an actual application to a race car wing which resulted in improved corner and straightaway speeds, an implication of increased down force (negative lift for the inverted airfoil) and lower drag. The second example was data from a low-speed wind tunnel. The results, shown in figure 1, indicated significant improvement in lift and drag for this airfoil geometry. The test was run at a Reynolds number of about 1 to 2×10^6.

To help explain the reason for the unexpected reduced drag, Liebeck hypothesized a flow field near the airfoil trailing edge with the Gurney flap. By comparing this with the flow field of the airfoil without the flap, he presented an explanation of the drag difference. The flow field near the trailing edge of a conventional airfoil is shown schematically in figure 2(a). According to reasoning described by Küchemann (e.g., refs. 2 and 3), the transport of the upper- and lower-surface boundary-layer vorticity along curved streamlines into the wake beyond the airfoil trailing edge induces velocities that have a component directed against the flow. If the boundary-layer vorticity is strong enough and the curvature due to trailing-edge angle is large enough, the retardation of the flow may cause it to separate. As a result, separation bubbles on the upper and lower surfaces may form, as shown in the figure. There is a wake momentum deficiency associated with this flow, which means that the pressure recovery obtained for an airfoil with unseparated flow is not realized in this case. This lack of pressure recovery implies higher drag for the airfoil with separated flow.

The hypothesized flow near the Gurney flap is shown schematically in figure 2(b). Liebeck's wind tunnel studies indicated turning of the flow over the back of the flap and reverse flow directly behind it. It was thought possible, therefore, that for airfoils with large enough trailing-edge angles, the wake momentum deficit is less for the flow with the Gurney flap than without it. Of course, as flap size is increased, the wake region size is correspondingly increased until the drag advantage of the flap no longer exists. An interesting feature of the hypothesized flow is the significant turning of the upper-surface trailing-edge flow, in terms of producing both increased lift due to turning and reduced form drag due to the longer region of attached flow near the trailing edge.

Roesch and Vuillet (ref. 4) discussed the application of similar devices to helicopter vertical stabilizers at a Reynolds number based on chord length R_c of 0.75×10^6. As would be expected, they found that lift C_L was increased and the angle for zero lift α_o was reduced while the lift-curve slope C_{L_α} was slightly increased. However, the drag for a trailing-edge strip of the same length as Liebeck's (1.25 percent of the local chord c, or $0.0125c$) was unchanged from the clean-wing value (i.e., no drag reduction). This lack of drag reduction was stated as possibly being due to the airfoil camber and the smaller relative thickness and trailing-edge angle of the airfoil they used. A larger strip ($0.05c$) showed a greater gain in maximum lift coefficient $C_{L,\max}$ but a significant drag increase also. (Liebeck stated in ref. 1 that flap lengths greater than about $0.0125c$ would probably show drag penalties relative to the clean wing.) Airfoil surface pressure data taken with the

0.05c strip indicated, at a given C_L, a large change in the trailing-edge flow field. (See fig. 3.) Of particular significance was a large suction effect on the upper surface near the trailing edge, an indication of a local curvature of the flow around the back side of the flap. This suction effect substantiated the finding of Liebeck that the flow turned over the back of the flap. Since the pressure gradient over the upper surface was milder for the airfoil with the trailing-edge device, it appears that much larger lift coefficients can be obtained before the flow separates.

Previously unpublished data taken in the Langley Low-Turbulence Pressure Tunnel show similar trends (private communication from Robert J. McGhee, Langley Research Center). An advanced-technology airfoil with a small trailing-edge (cusp-like) angle was tested at $R_c = 3 \times 10^6$ with a 0.0125c-length Gurney flap. Force data indicate substantial lift increases but also very large drag penalties at low and moderate lift coefficients (fig. 4). Pressure-distribution data (fig. 5) near the trailing-edge region show the flow field to be affected in a manner similar to the results of Roesch and Vuillet (ref. 4) mentioned previously. A suction increase on the upper surface and pressure increase on the lower surface indicate a downward turning of the flow compared with the clean airfoil.

A wind tunnel study of modifications made to an aircraft airfoil section was conducted by Sewall, McGhee, and Ferris (ref. 5) at $R_c = 10 \times 10^6$. Changes in the trailing-edge geometry yielding an effective camber increase (similar to what a Gurney flap does) created lift, drag, and trailing-edge pressure-distribution changes of the same type shown in figure 5.

From this review of research results, it appears that an increase in lift can be expected from a device similar to a Gurney flap independent of airfoil section geometry. This increase is most likely due to the effective increase in trailing-edge camber afforded by the device. However, the potential benefits in terms of drag may be limited to airfoil sections with relatively large trailing-edge closure angles or high wing lift coefficients or both.

The present study provides insight into the flow mechanism. The hypothesized flow field is substantiated from a visual portrayal of the flow structure near the Gurney flap. In addition, the effects of flap geometry changes are indicated.

Symbols

AR	wing aspect ratio, $\frac{b^2}{S}$
b	wing span, m (ft)
C_D	drag coefficient, $\frac{\text{Drag}}{q_\infty S}$
C_L	lift coefficient, $\frac{\text{Lift}}{q_\infty S}$
$C_{L,\max}$	maximum lift coefficient
C_{L_α}	lift-curve slope, $\frac{dC_L}{d\alpha}$, deg^{-1}
C_p	pressure coefficient, $\frac{p - p_\infty}{q_\infty}$
c	wing or airfoil chord, m (ft)
p	static pressure, Pa (lbf/ft^2)
p_∞	free-stream static pressure, Pa (lbf/ft^2)
q_∞	free-stream dynamic pressure, $(1/2)\rho_\infty U_\infty^2$, Pa ($\text{lbf/ft}^2$)
R	unit Reynolds number, $\frac{U_\infty}{v}$, m^{-1} (ft^{-1})
R_c	Reynolds number based on chord length, $\frac{U_\infty c}{v}$
S	wing area, m^2 (ft^2)
U_∞	free-stream velocity, m/sec (ft/sec)
x	dimension in wing chordwise direction, m (ft)
$(x/c)_{\text{sep}}$	nondimensional location of flow separation
y	dimension in wing spanwise direction, m (ft)
α	wing or airfoil angle of attack, deg
α_o	angle of attack at zero lift, deg
ρ_∞	free-stream density, kg/m^3 (lbm/ft^3)
v	kinematic viscosity, m^2/sec (ft^2/sec)

Test Setup and Method

Test Facility

The Langley 16- by 24-Inch Water Tunnel is shown in figure 6. The tunnel has a vertical test section with an effective working length of about 1.37 m (4.50 ft). The velocity in the test section can be varied from 0 to 0.23 m/sec (0.75 ft/sec), which results in Reynolds numbers from 0 to 2.54×10^5 m^{-1} (7.73×10^4 ft^{-1}) based on summer water temperatures of 25.6°C (78°F). The normal test velocity yielding smooth flow is 0.076 m/sec (0.250 ft/sec), which results in Reynolds numbers of

8.46×10^4 m^{-1} (2.58×10^4 ft^{-1}) at 25.6°C (78°F) and 7.51×10^4 m^{-1} (2.29×10^4 ft^{-1}) at 20°C (68°F).

The model support system has deflection ranges of ±33° and ±15° in two planes of rotation. Rotation is accomplished via electronic remote control and visual indicators allow the user to set angles within about ±0.25°.

The flow visualization method for this investigation used colored dye injected from overhead-mounted 0.107-cm (0.042-in.) stainless-steel probes and dye injected from orifices installed on the model wing surface.

Models

The Gurney flap models were made of 0.16-cm (1/16-in.) thick rubber strips that spanned the trailing edge of the wing. The models were tested by attaching the strips to the lower-surface trailing edge, perpendicular to the chord line of a rectangular wing. The wing had an NACA 0012 airfoil, an aspect ratio of 6.7, a span of 38.1 cm (15.0 in.), and a chord of 11.4 cm (4.5 in.). This was a semispan model mounted at its root chord to a long, narrow support strut. (See fig. 7.)

The four Gurney flap geometries tested are shown in figure 8. The flap in figure 8(a) is, at 0.015c, slightly larger than the one tested by Liebeck (ref. 1). The other three Gurney flap configurations (figs. 8(b), 8(c), and 8(d)) are longer (0.042c, 0.042c, and 0.055c). The longer flaps were tested to help visualize the flow resulting from larger recirculation regions and to see what effect size variation had on the flow over the wing trailing edge. The Gurney flap with the pressure side filled in (fig. 8(c)) was tested to see if a configuration that might be easier to apply to a wing would change the effectiveness of the flap. The serrated flap was studied to see the effects of the generation of a more complex flow through the serrations.

Test Method

The tests were run at a free-stream velocity U_∞ of 0.076 m/sec (0.250 ft/sec). For most of the tests, the water temperature in the tunnel stabilized at 20°C (68°F), which gave a Reynolds number of 7.51×10^4 m^{-1} (2.29×10^4 ft^{-1}). Based on the wing chord, the test Reynolds number was 8588. When the test section flow was stabilized at the test velocity, the model was set to the desired attitude. In the present tests, dye was introduced into the flow from above the model. The dye streak position was adjusted so that it met the model at the leading-edge stagnation point and split to flow along the wing upper and lower surfaces simultaneously. The spanwise location was at 33 percent of the semispan from the wing root. In addition, dye was introduced above the wing upper surface to show the flow field away from the wing surface. A laser sheet was also used to visualize the oscillatory laminar wake. An argon laser with appropriate optics to spread the beam into a sheet was used to excite a fluorescein dye.

Flow visualization data were recorded using still color photography. Still photographs were taken on 70-mm color negative film and printed in an 8- by 10-in. form. A set of close-up lenses allowed photographs to be taken as close as 30.5 cm (12.0 in.) from the area of interest to allow analysis of small, detailed flow structures.

Only one camera was used, and generally all attitudes were recorded at one viewpoint. The camera was then moved to a new viewpoint and the model was returned to its original position to avoid any effects of hysteresis that might result from changing the model attitude in reverse direction. In addition, after the attitude was changed, a pause of several seconds was necessary to allow effects of the dynamic response of the flow field to the change to dissipate. An example of this for the Gurney flap models was the regions of highly concentrated vorticity that were shed from the trailing-edge region when an increase in angle of attack was made.

When all the desired visual data were recorded, any areas of specific interest were reexamined to check for repeatability and to analyze any phenomena that may have been difficult to interpret or resolve using the recording media. This was of particular interest for regions of the flow that were too small to accurately record and for aspects of the flow whose unsteady nature could not be conveyed appropriately on film. When analyzing these results, remember that separation onset will be observed at much lower angles of attack than would be expected for flows at higher Reynolds numbers.

Analysis and Discussion

The analysis of the test results has been done with color photographs used as the primary data. From these photographs, the nondimensional location of separation $(x/c)_{sep}$ of the flow from the upper surface of the wing was determined. Three criteria were used for visually determining the separation location: the point of obvious (abrupt) dye separation from the surface (fig. 9(a)), the point at which a change in the curvature (change in smoothly varying slope implies change in the second derivative d^2y/dx^2) of the dye over the wing surface occurred (fig. 9(b)), or, from the wing trailing edge forward, the point where

the separated dye and its shadow on the wing surface merged (fig. 9(c)). Although these criteria may not be rigorously defendable as exact signs of separation, they were visually associated with separation and provided a consistent indication for such determinations. They were not all observable for every situation and they did not always show a distinct separation point. However, through observation of the separation locations at lower and higher angles of attack, the general area of separation could be identified and the location subsequently estimated. Approximate accuracies of the locations were on the order of $\pm 0.02c$.

Baseline Wing

The baseline configuration was a rectangular wing with a clean trailing edge. Flow visualization photographs of the wing at $\alpha = 0°$ and 2° are shown in figures 10(a) and 10(b), respectively. At $\alpha = 0°$, the separation location on the wing upper surface was at about $0.69c$ ($(x/c)_{sep} = 0.69$) from the leading edge. At $\alpha = 2°$, the separation moved forward to about $(x/c)_{sep} = 0.53$. Clearly, the boundary layers on the wing at this low Reynolds number cannot tolerate the pressure gradients imposed on them. Another feature of these low Reynolds number flows is the oscillatory wake that is characteristic of laminar flow behind these wings. The laminar wake shed by the clean wing in this study is shown in figure 11 as visualized by a laser light sheet. The light sheet was generated to be parallel to the free-stream flow, yielding a cross-sectional view of the wake. Such an oscillatory wake behind an airfoil was visualized in an NACA smoke tunnel by Jacobs and Sherman (ref. 6). In addition, the excellent flow visualizations by Freymuth in accelerating flows show very distinct vortical regions in airfoil wakes at lower free-stream speeds (ref. 7). As speed increases, these organized flows break down into turbulence. Tyler, in reference 8, tested airfoils in water and air and made extensive measurements of the wake oscillations at angles of attack from 0° to 90°. The separation locations on the upper surface of all the models, at all attitudes tested, remained constant at each attitude and did not oscillate as the wake did.

Wing With Small Gurney Flap ($0.015c$)

The progression of separation is shown at three angles of attack for the wing with the small Gurney flap in figure 12. The flow over the wing with the small Gurney flap at $\alpha = 0°$ separated from the upper surface at $(x/c)_{sep} = 0.83$. This represents an improvement over the clean wing, which had a separation location of $(x/c)_{sep} = 0.69$ at $\alpha = 0°$. At $\alpha = 2°$, however, the wing with the small Gurney flap and the clean wing had separation locations roughly at $(x/c)_{sep} = 0.54$ and 0.53, respectively. This indicates that the small Gurney flap became ineffective as the adverse pressure gradient in the trailing-edge region increased with increasing α. The global pressure field quickly dominated the local flow in the region of the Gurney flap. Figure 12(b), which shows the flow visualized by dye on the surface at $\alpha = 1°$, indicates a gradual spanwise migration of flow apparent in the separated region.

Wing With Large Gurney Flap ($0.042c$)

To help better visualize the flow in the region aft of the Gurney flap, a larger size ($0.042c$) was tested. The flow over the upper surface did not begin to separate until $\alpha = 2°$. At this α, the separation location was at $0.99c$ from the leading edge (fig. 13(a)). At $\alpha = 5°$ (fig. 13(b)) the separation location $(x/c)_{sep}$ was 0.31, which shows that even at this relatively high α (highest α tested) the large Gurney flap still had a stronger effect on the flow than did the small Gurney flap, for which $(x/c)_{sep} = 0.2$ at $\alpha = 5°$. Again, there was a gradual spanwise movement of the flow near the separation, as indicated by the widening of the region marked by dye.

Wing With Large Gurney Flap ($0.042c$) and Pressure Side Filled In

As previously mentioned, an actual wing design might require that the region on the wing lower surface forward of the Gurney flap be filled in as shown in figure 8(c). Such a configuration was tested in the water tunnel to see if there was any effect on the flow separation locations. At the lower angles of attack ($\alpha < 3°$), the separation locations for this configuration were similar to those for the large Gurney flap. At $\alpha = 3°$ (fig. 14(a)), $(x/c)_{sep} = 0.64$ versus $(x/c)_{sep} = 0.72$ for the large Gurney flap. At $\alpha = 3.5°$ for this configuration (fig. 14(b)), $(x/c)_{sep} = 0.32$. This was also less than the separation location $(x/c)_{sep} = 0.46$ for the large Gurney flap when the wing was at $\alpha = 3.5°$, and it was almost equivalent to $(x/c)_{sep} = 0.31$ for the large Gurney flap at $\alpha = 5°$. It therefore appears that there may have been some slight degradation in performance with the pressure side filled in, since we have changed the flow phenomena. Parametric studies of the geometry of the filled-in region may reveal a more efficient configuration.

Wing With Large Serrated Gurney Flap

The serrated Gurney flap was investigated to determine the effect that the complicated flow induced by the serrations had on the flow around the wing.

The dye flow at two angles of attack is shown in figure 15. The locations of upper-surface flow separation found using this device were farther forward of the trailing edge than those found using the large Gurney flap. They were, however, farther aft than those for the small Gurney flap. Intuitively this is not surprising. Although this was a larger flap ($0.055c$), it is likely that the cutouts forming the serrations allowed fluid to pass through, preventing a large recirculation region to form on the back side of the flap. This lack of recirculation is evident in figure 15(a). The dye that accumulated on the pressure side of the wing forward of the flap is passing through and forming streaks along the wing trailing edge. In addition, small "curly" vortices were formed that had near-streamwise rotation vectors. These vortices (shown schematically in fig. 16) were quickly stretched and "absorbed" by the large alternating vortices shed from the trailing edge. It was felt that these axial vortices might induce the trailing-edge boundary layer to remain attached longer, but the adverse pressure gradient apparently overwhelmed any beneficial effect they might have at this Reynolds number.

Comparison of Separation Results

The nondimensional separation locations as a function of angle of attack for the five configurations tested are shown in figure 17. The data for the clean wing are almost linear and should represent the forward limit for separation at this Reynolds number for all configurations using this wing. The effect of the Gurney flap in all cases was to move the separation position aft at $\alpha = 0°$. As α increased, however, the distinction between the configurations became evident. As is well known, as α is increased, the adverse pressure gradient on the rear portion of the wing upper surface strengthens. This environment generally makes it increasingly difficult for the boundary layer to remain attached. The low Reynolds number at which these models were tested made the flow over the wing surface very sensitive to the pressure recovery over the aft part of the wing. The flow visualization indicates that the flow induced by the large Gurney flaps delayed the onset of separation best. Eventually, however, all the configurations were dominated by the adverse effects of increasing α and the data fall near the clean-wing separation line in figure 17.

Details of the Flow Field Near the Gurney Flap

The flow in the region near the wing trailing edge is shown in the photographs in figure 18. Figures 18(a) and 18(b) show the recirculation region behind the Gurney flap as it oscillates under the influence of the vortices shed from the wing lower and upper surfaces. The schematic in figure 18(c) shows the motion observed inside the recirculation region. The flow loops that were marked by dye moved in the directions shown by the arrows. Each loop only moved, however, when the opposite-side wing vortex was shedding. The loop in the left part of the recirculation region moved when the upper surface vortex was shedding, as shown in the schematic of figure 18(c). The region was divided in the middle. The region of accumulated dye in front of the Gurney flap also indicated a recirculation region. This agrees with the flow field as Liebeck hypothesized it in reference 1.

Concluding Remarks

A flow visualization test of a series of Gurney flap configurations has been conducted in the Langley 16- by 24-Inch Water Tunnel at a Reynolds number of 8588. The purpose of the study was to investigate visually the flow field near a Gurney flap to enable definition of the flow structure. In addition, the effects of the flaps on wing upper-surface flow separation were examined. The objectives of the test were met and the following conclusions may be drawn:

1. The visualization results indicated that the flow field hypothesized by Liebeck was generally substantiated.
2. The different Gurney flap geometries had favorable effects on wing upper-surface flow separation at angles of attack less than 3.5°. The most favorable effects were found with the larger flaps.
3. The effects of Gurney flaps on lift and pressure distributions reported in previous research imply an effect on the flow field that was substantiated by the current test.

It is important to note that previous wind tunnel research was done at Reynolds numbers on the order of 10^6. The water tunnel studies reported herein were made at Reynolds numbers several orders of magnitude lower. Clearly the boundary layer and wake characteristics differ between the two mediums. Therefore, the separation locations of the flows in the two mediums will differ (i.e., the location of flow separation at a given angle of attack). However, the general effects of the trailing-edge devices on the flow are the same, since an effective increase in camber provides an inviscid effect to the first order (i.e., camber accelerates the flow over the upper surface). In these tests, the flow field induced by the Gurney flap was simulated in a qualitative way.

References

1. Liebeck, Robert H.: Design of Subsonic Airfoils for High Lift. *J. Aircr.*, vol. 15, no. 9, Sept. 1978, pp. 547–561.
2. Küchemann, D.: *Inviscid Shear Flow Near the Trailing Edge of an Aerofoil.* Tech. Rep. 67068, British Royal Aircraft Establ., Mar. 1967.
3. Küchemann, D.: *The Aerodynamic Design of Aircraft.* Pergamon Press, c.1978.
4. Roesch, Philippe; and Vuillet, Alain: New Designs for Improved Aerodynamic Stability on Recent Aerospatiale Helicopters. *Vertica*, vol. 6, no. 3, 1982, pp. 145–164.
5. Sewall, W. G.; McGhee, R. J.; and Ferris, J. C.: Wind-Tunnel Test Results of Airfoil Modifications for the EA-6B. *Technical Papers—Fifth AIAA Applied Aerodynamics Conference,* Aug. 1987, pp. 248–256. (Available as AIAA-87-2359.)
6. Jacobs, Eastman N.; and Sherman, Albert (appendix by Ira H. Abbott): *Airfoil Section Characteristics as Affected by Variations of the Reynolds Number.* NACA Rep. 586, 1937.
7. Freymuth, Peter: The Vortex Patterns of Dynamic Separation: A Parametric and Comparative Study. *Prog. Aerosp. Sci.*, vol. 22, no. 3, 1985, pp. 161–208.
8. Tyler, E.: Vortex Formation Behind Obstacles of Various Sections. *Philos. Mag.*, ser. 7, vol. 11, no. 72, Apr. 1931, pp. 849–890.

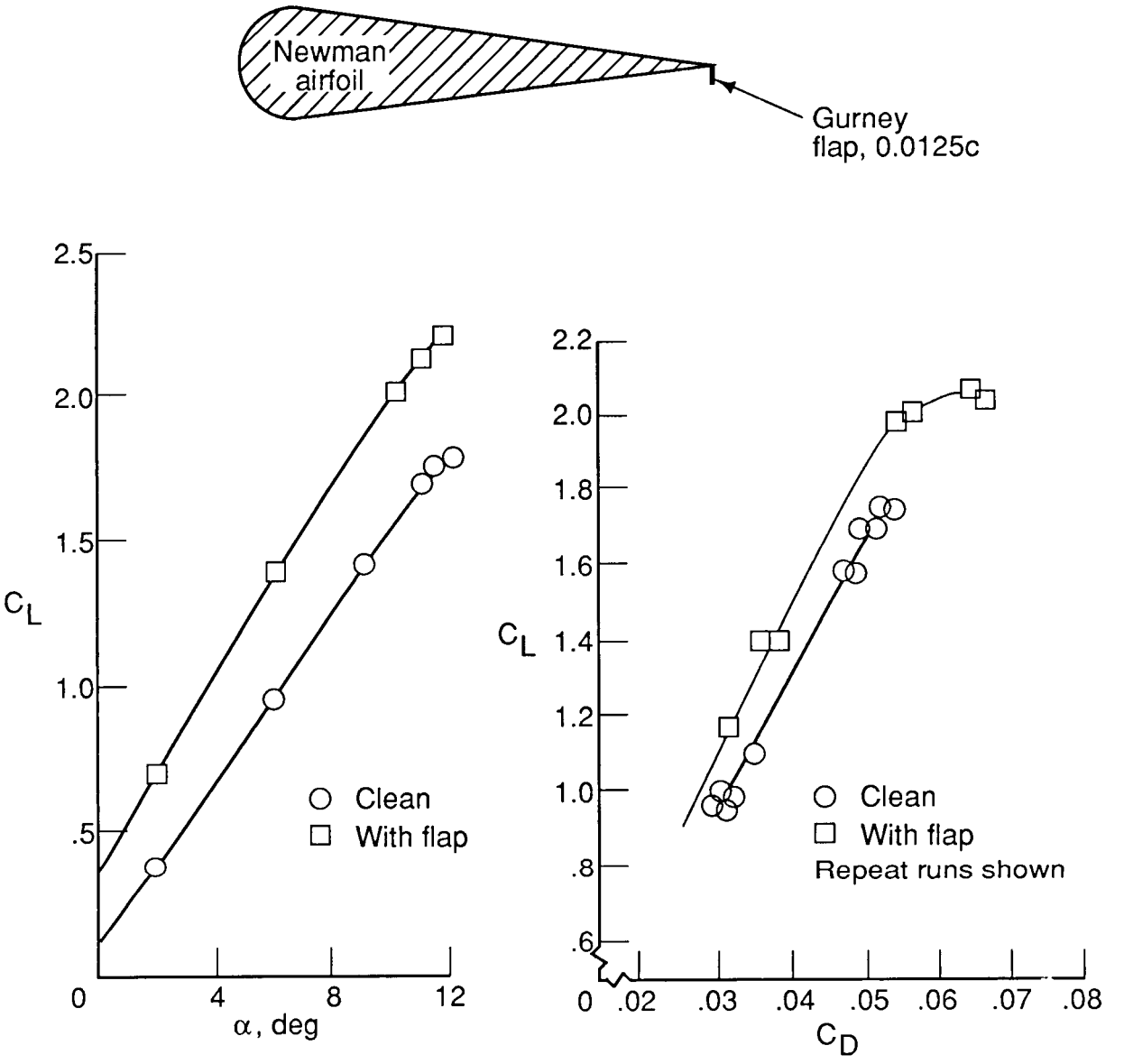

Figure 1. Gurney flap geometry and wind tunnel results. $R_c = 1$ to 2×10^6. (From ref. 1. Copyright AIAA. Reprinted with permission.)

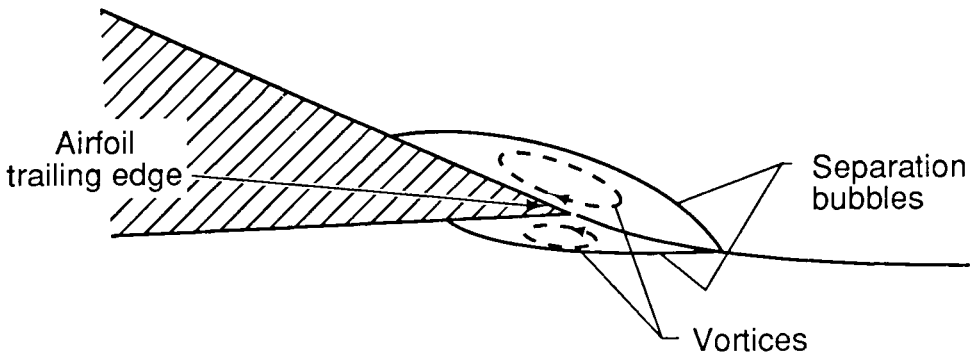

(a) Conventional airfoil at moderate C_L.

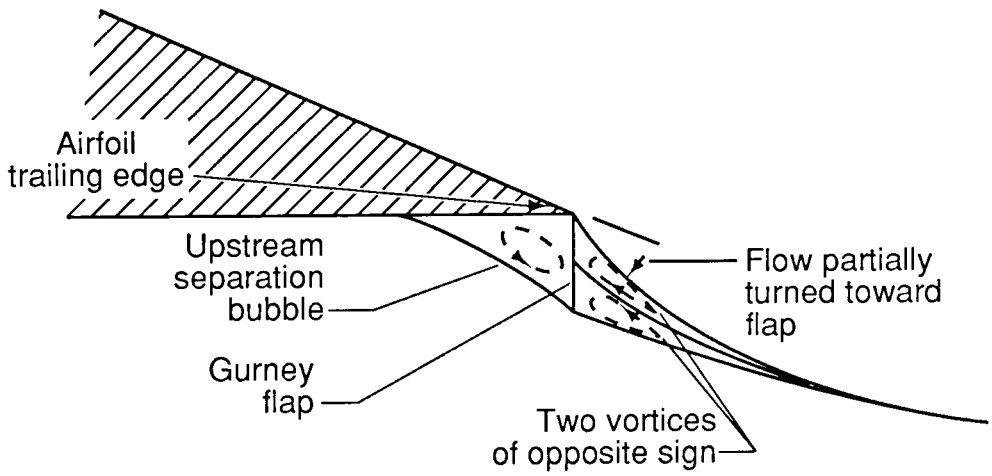

(b) Hypothesized flow near Gurney flap.

Figure 2. Trailing-edge flow fields. (From ref. 1. Copyright AIAA. Reprinted with permission.)

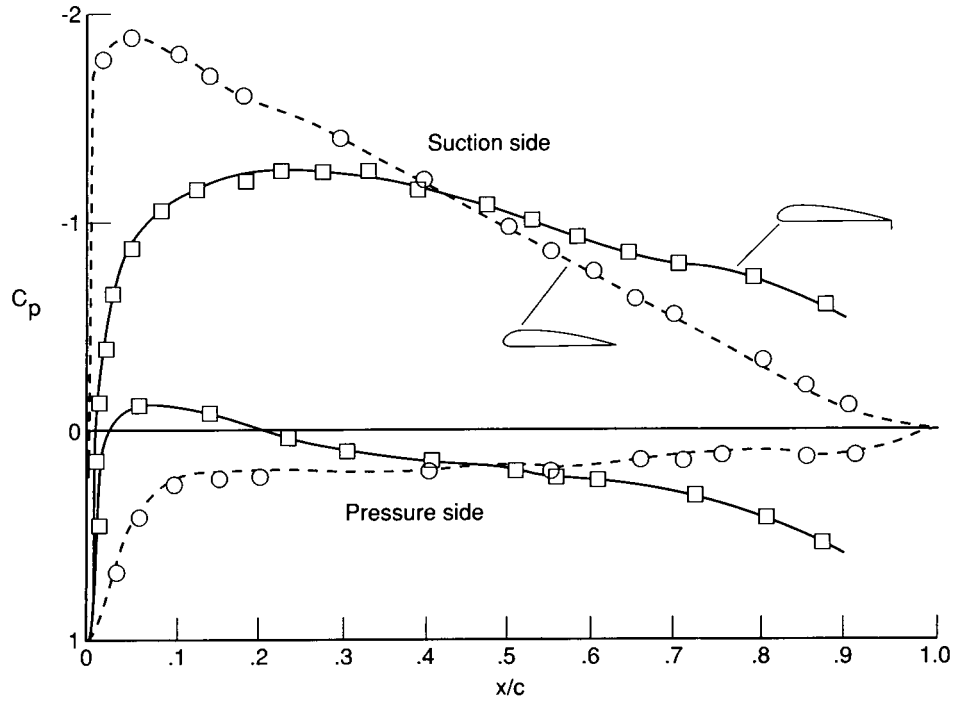

Figure 3. Airfoil surface pressure data. $AR = 5$; $C_L = 1.07$; $R_c = 0.75 \times 10^6$; $y/b = 0.5$. (From ref. 4. Copyright Pergamon Press, Inc. Reprinted with permission.)

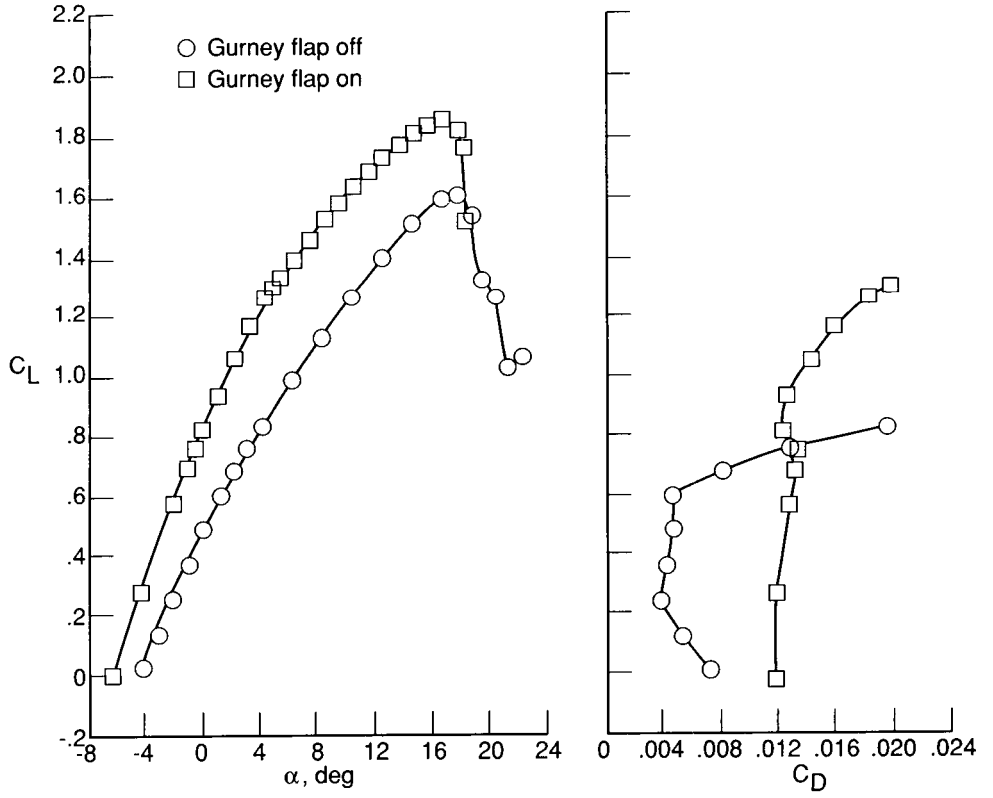

Figure 4. Force data for advanced-technology airfoil. $R_c = 3 \times 10^6$.

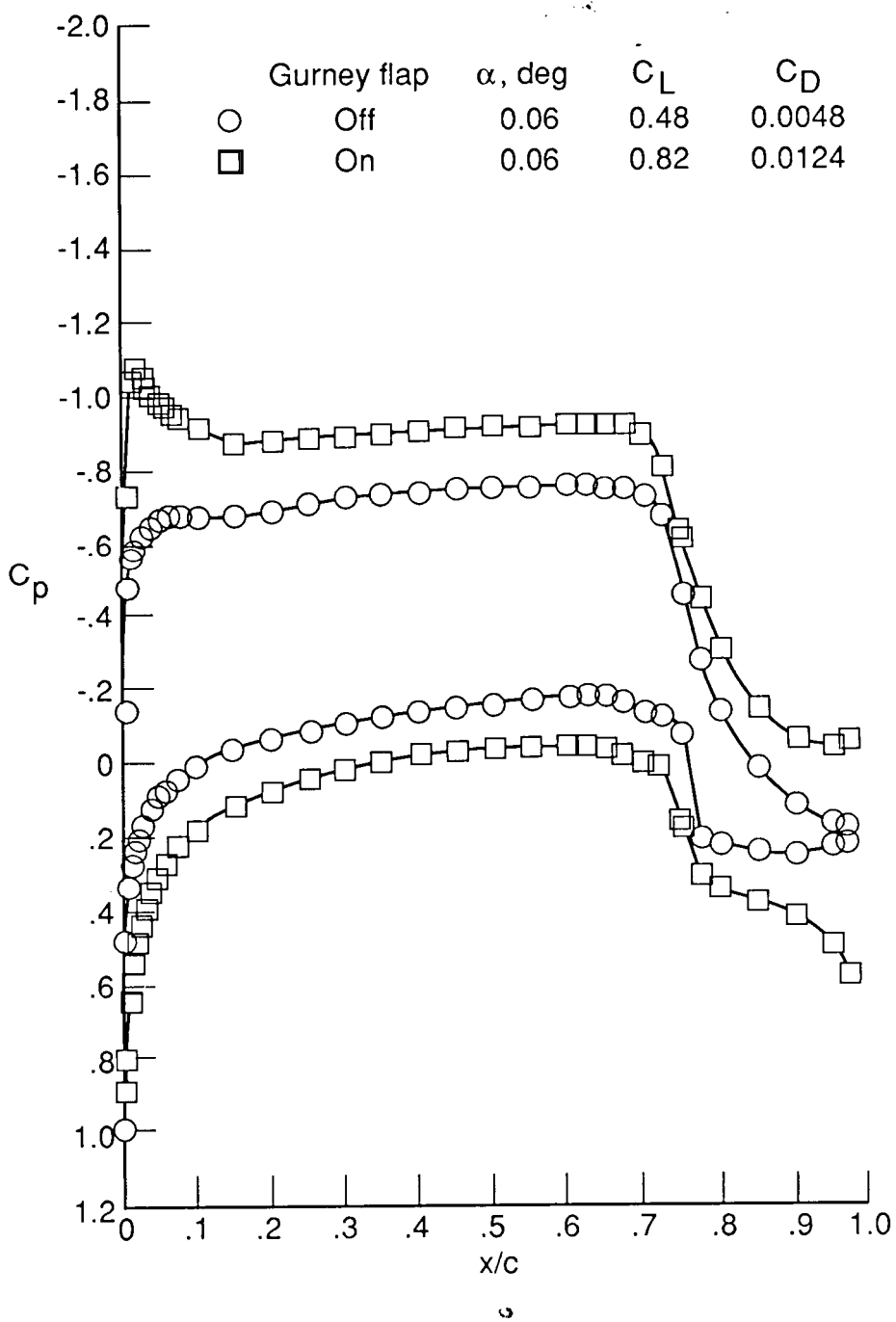

Figure 5. Surface pressure data for advanced-technology airfoil. $R_c = 3 \times 10^6$.

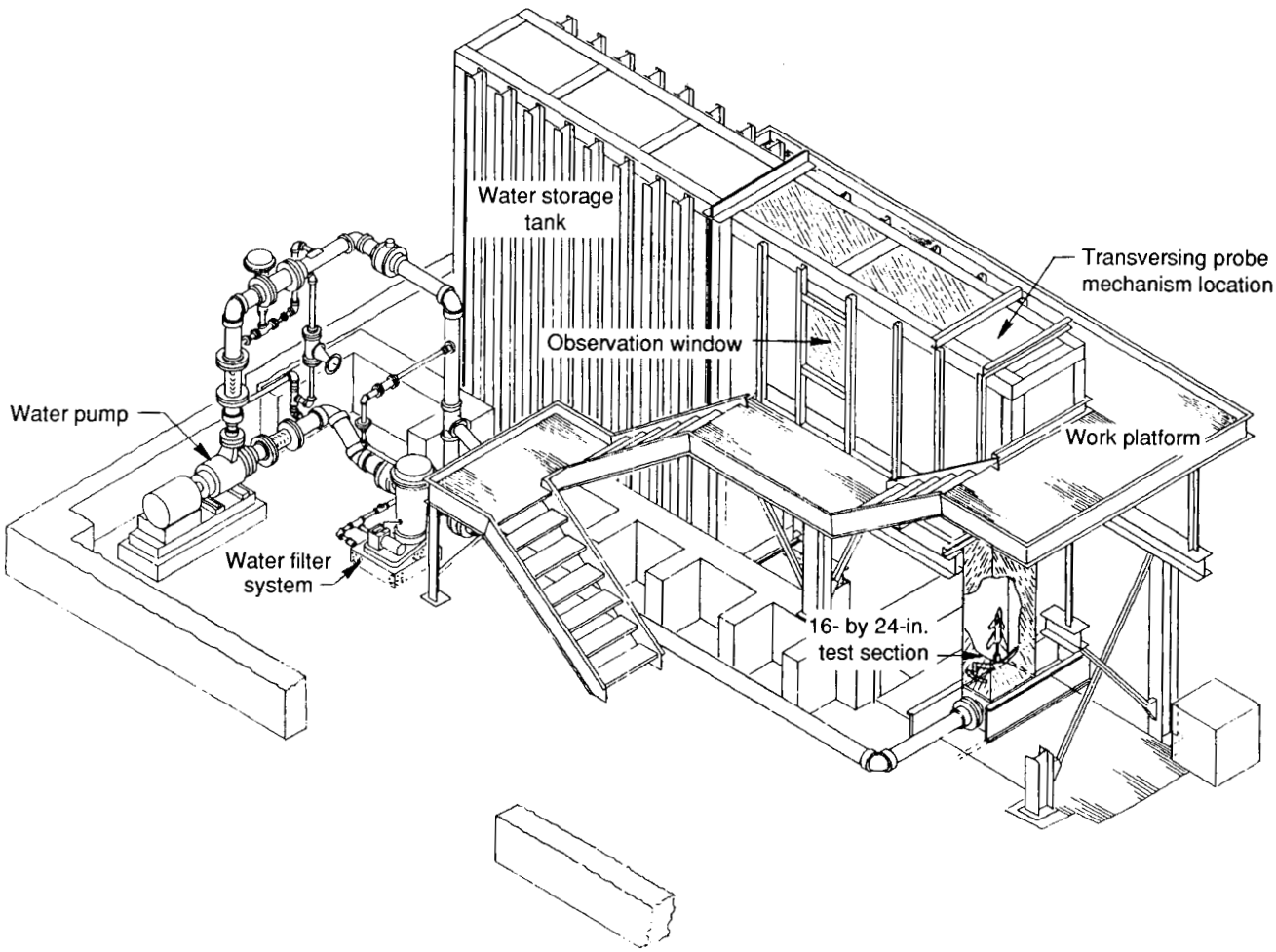

Figure 6. Langley 16- by 24-Inch Water Tunnel.

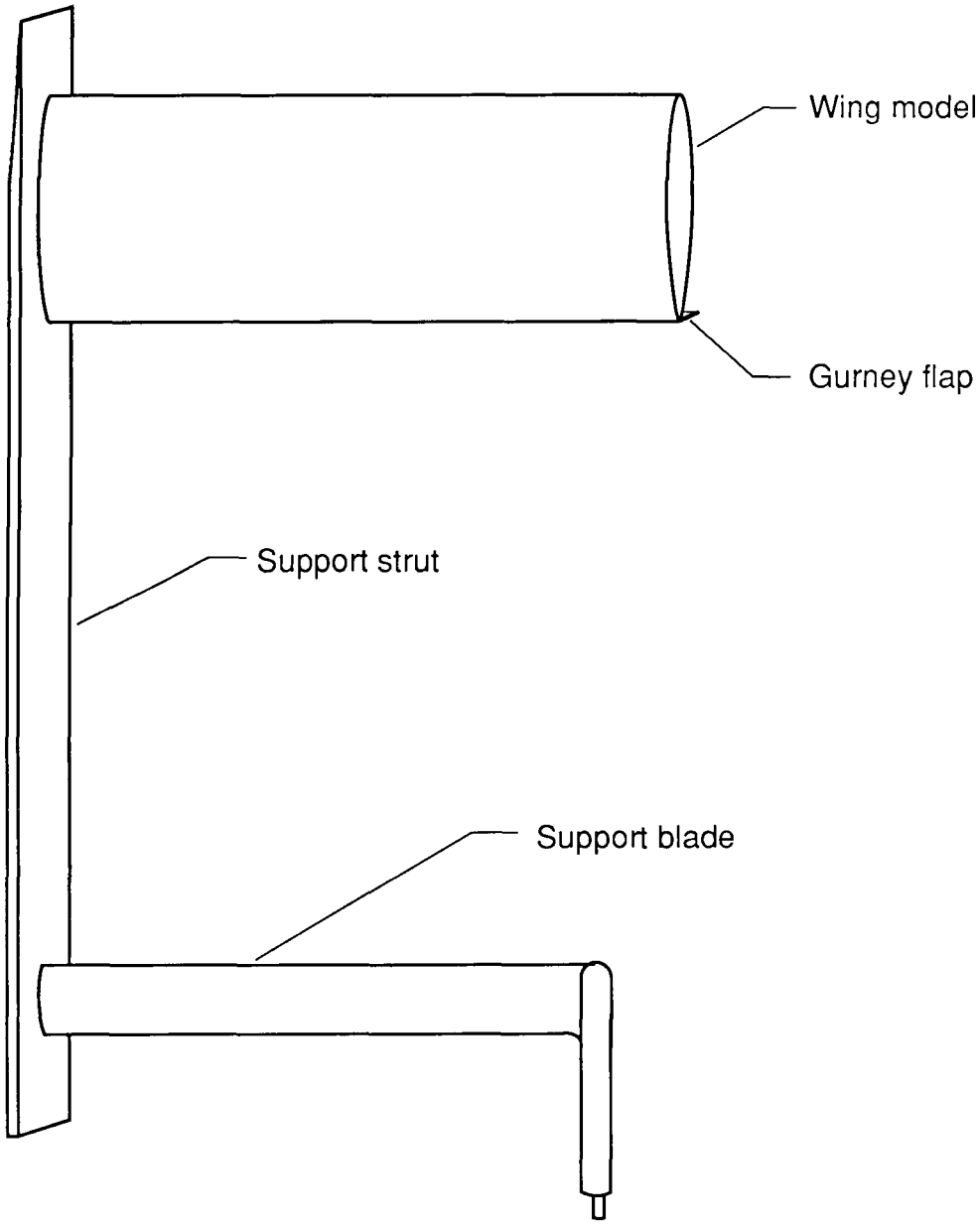

Figure 7. Wing model mounted to support structure.

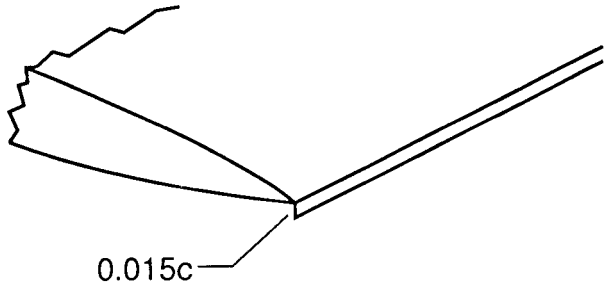

(a) Small Gurney flap.

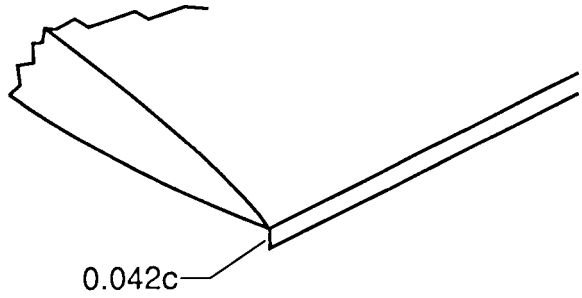

(b) Large Gurney flap.

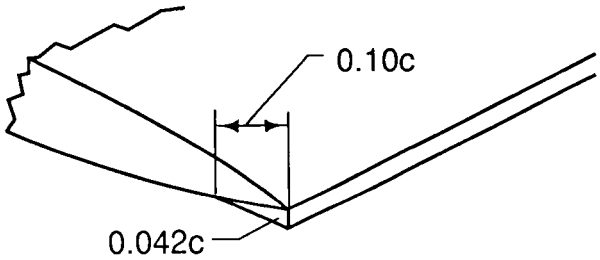

(c) Large Gurney flap, pressure side filled in.

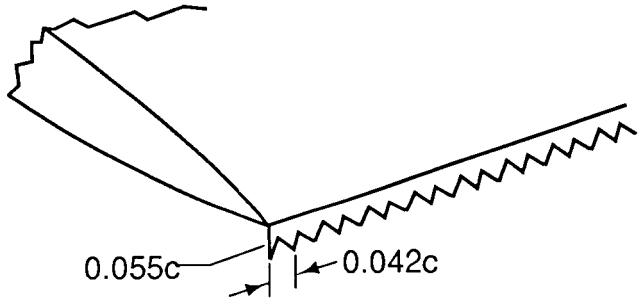

(d) Large Gurney flap, serrated.

Figure 8. Gurney flap models tested.

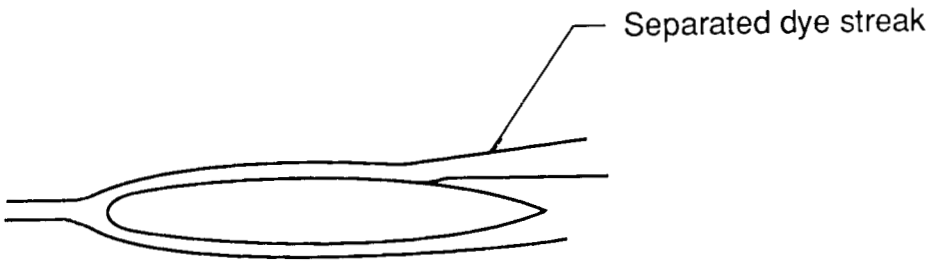

(a) Dye separation from surface.

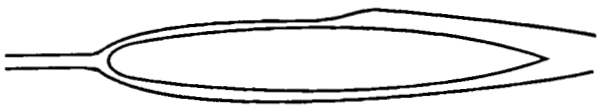

(b) Change in curvature of dye surface.

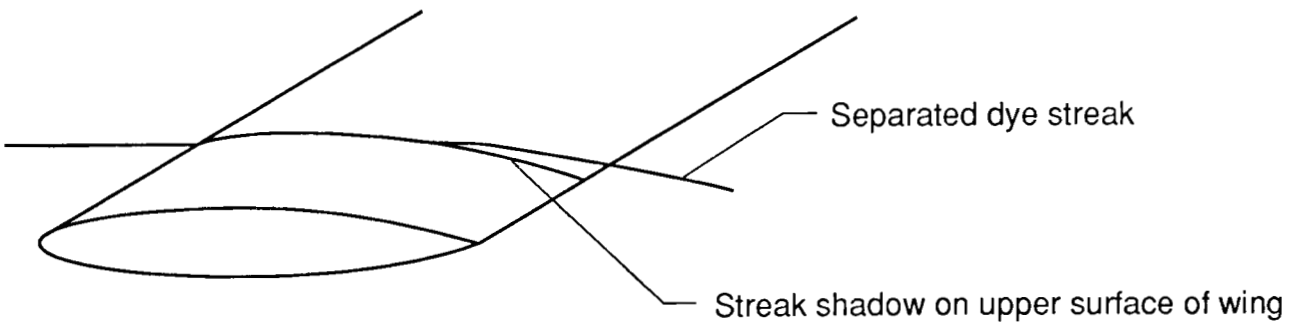

(c) Merging of dye streak and its shadow.

Figure 9. Visual criteria for determination of separation location.

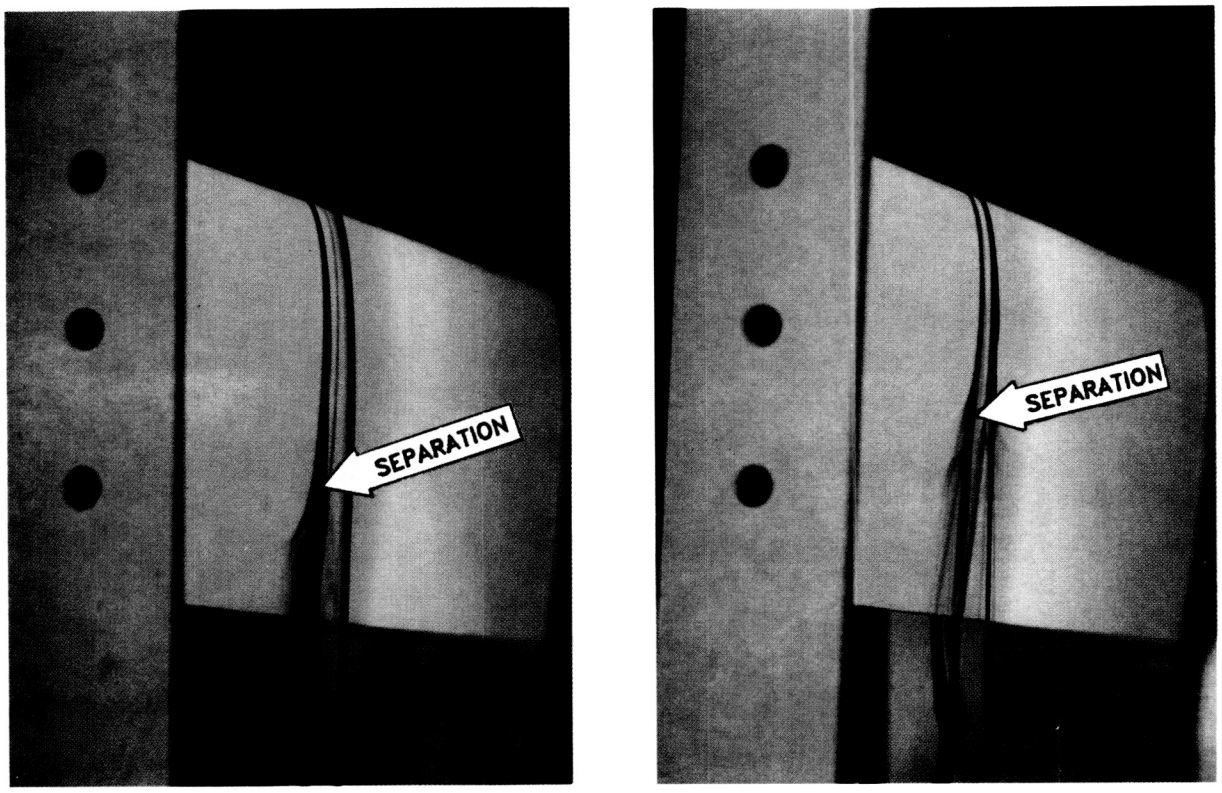

L-87-2821 L-87-2823

(a) $\alpha = 0°$. (b) $\alpha = 2°$.

Figure 10. Rectangular wing with clean trailing edge.

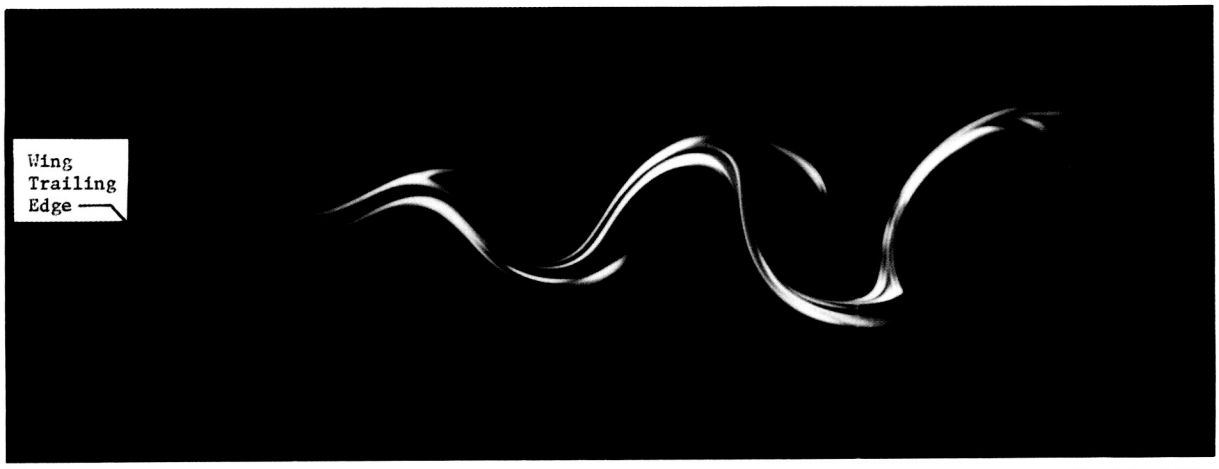

L-87-10,952

Figure 11. Laminar wake behind clean wing.

ORIGINAL PAGE
COLOR PHOTOGRAPH

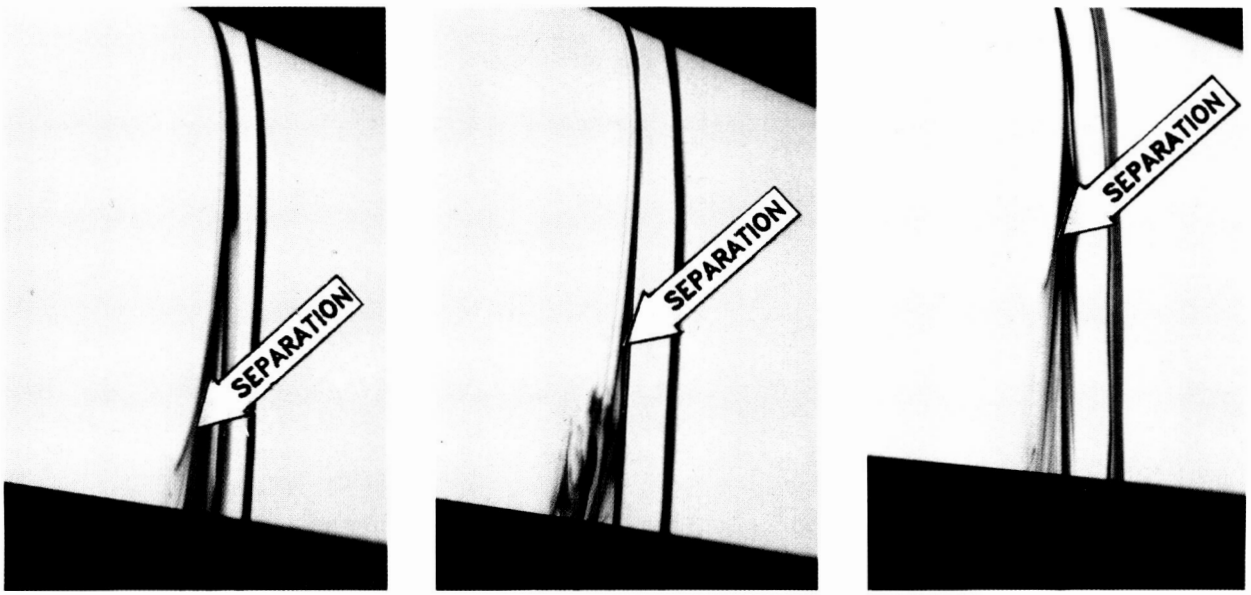

L-87-3461 L-87-3458 L-87-3466

(a) $\alpha = 0°$. (b) $\alpha = 1°$. (c) $\alpha = 2°$.

Figure 12. Rectangular wing with small Gurney flap.

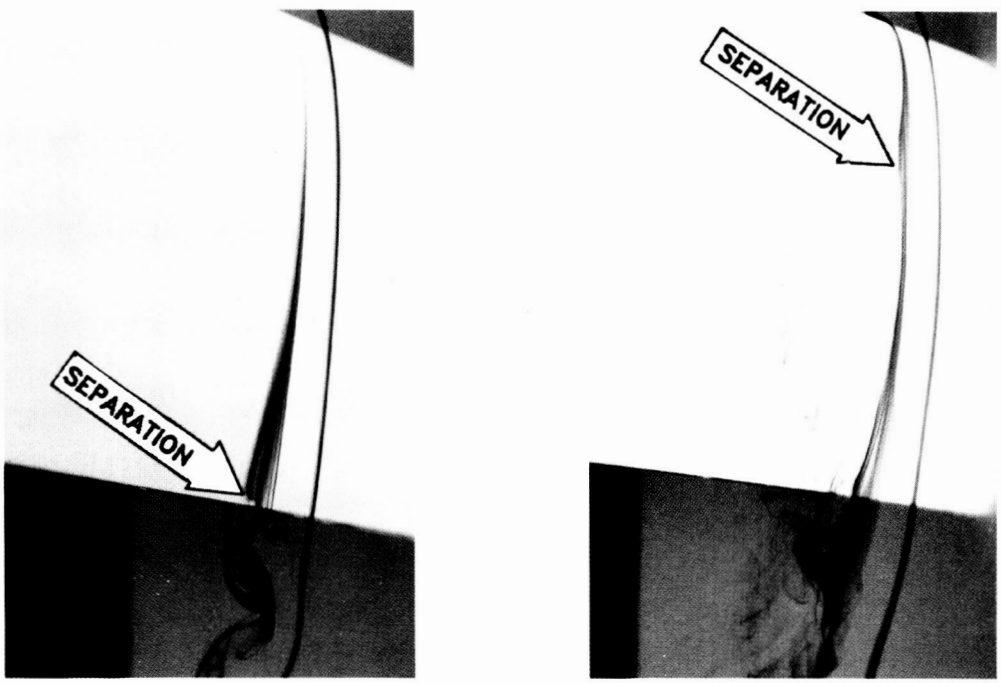

L-87-3358 L-87-3377

(a) $\alpha = 2°$. (b) $\alpha = 5°$.

Figure 13. Rectangular wing with large Gurney flap.

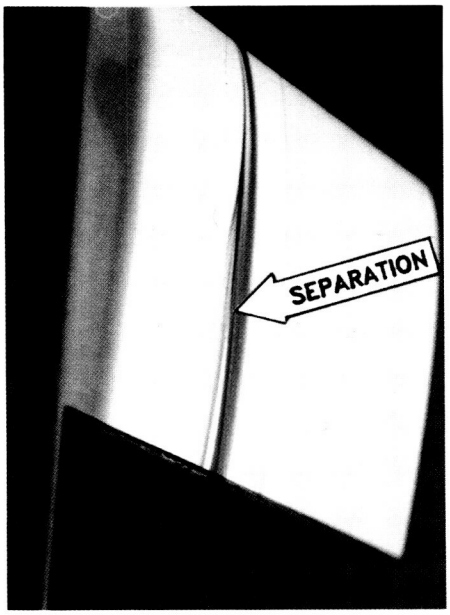

L-87-3661

(a) $\alpha = 3°$.

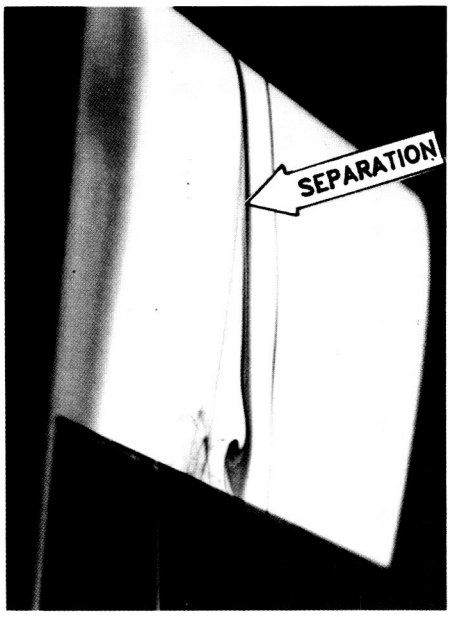

L-87-3654

(b) $\alpha = 3.5°$.

Figure 14. Rectangular wing with filled-in region ahead of large Gurney flap.

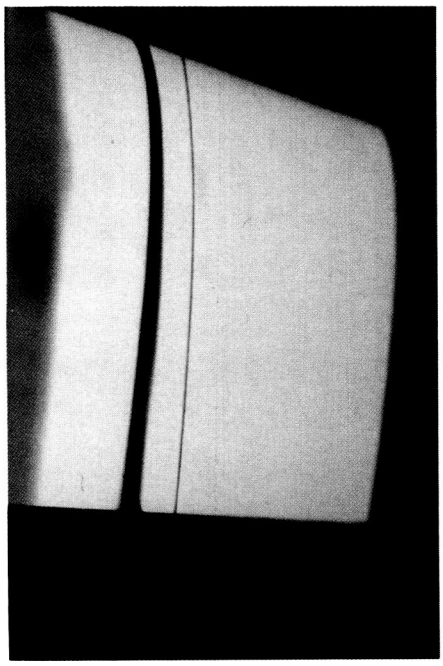

L-87-3673

(a) $\alpha = 0°$.

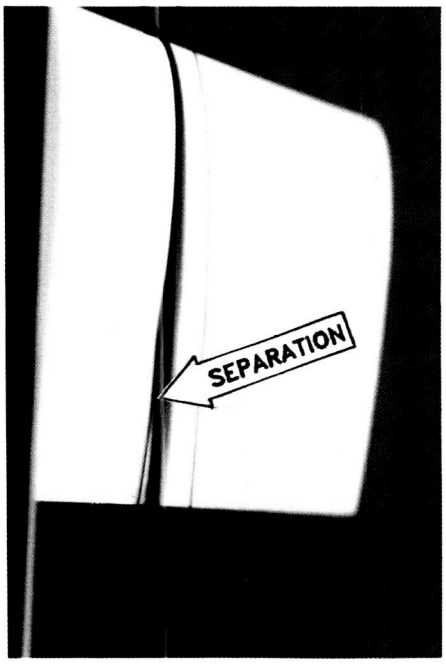

L-87-3669

(b) $\alpha = 2°$.

Figure 15. Rectangular wing with serrated Gurney flap.

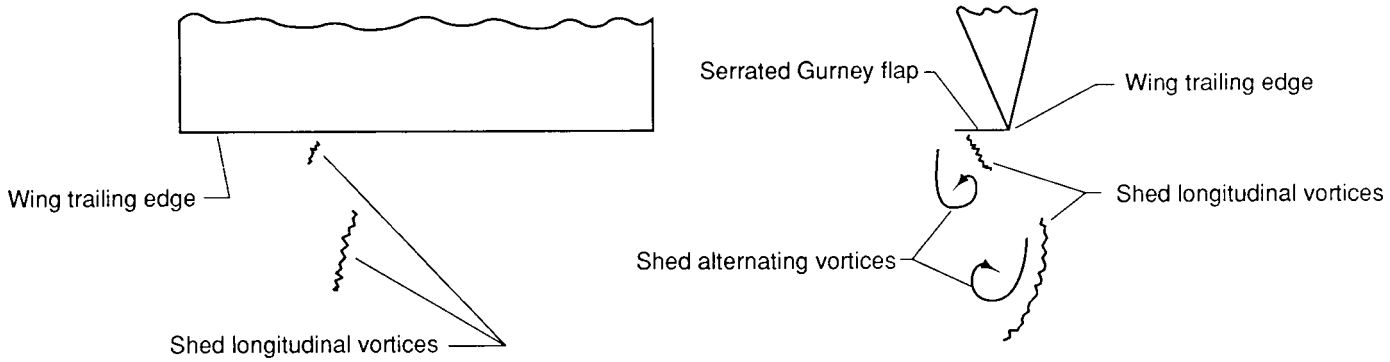

(a) Wing plan view.

(b) Wing trailing-edge region, side view.

Figure 16. Longitudinal vortices shed behind serrated Gurney flap.

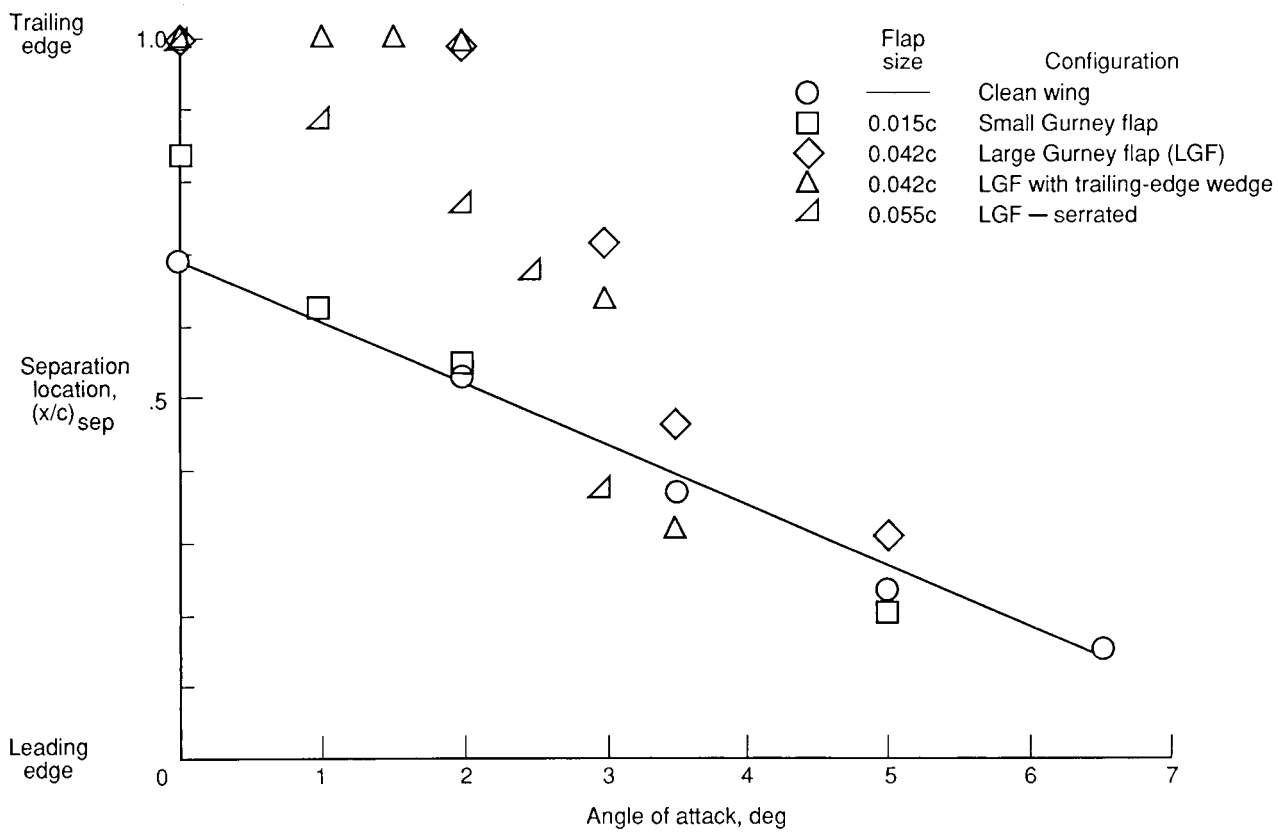

Figure 17. Nondimensional separation locations for clean wing and wing with various Gurney flap configurations.

ORIGINAL PAGE
COLOR PHOTOGRAPH

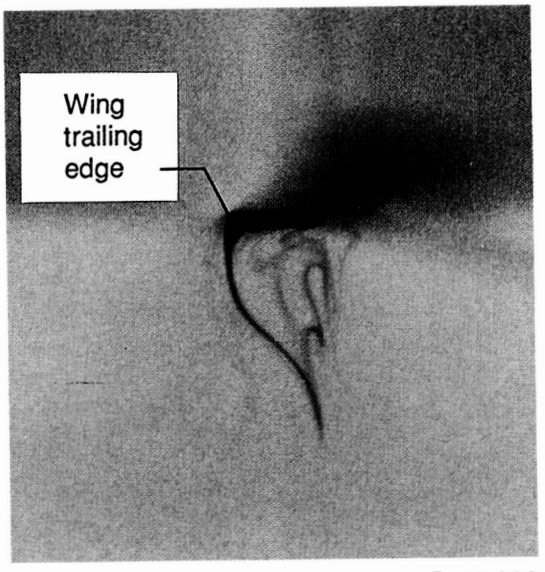

L-88-206

(a) Lower-surface vortex shedding.

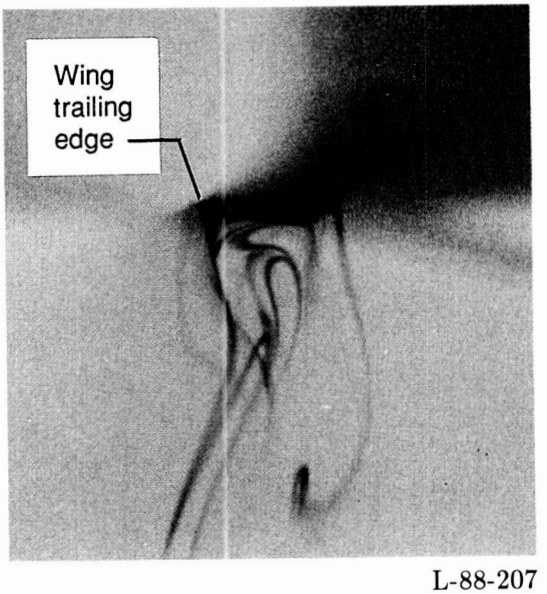

L-88-207

(b) Upper-surface vortex shedding.

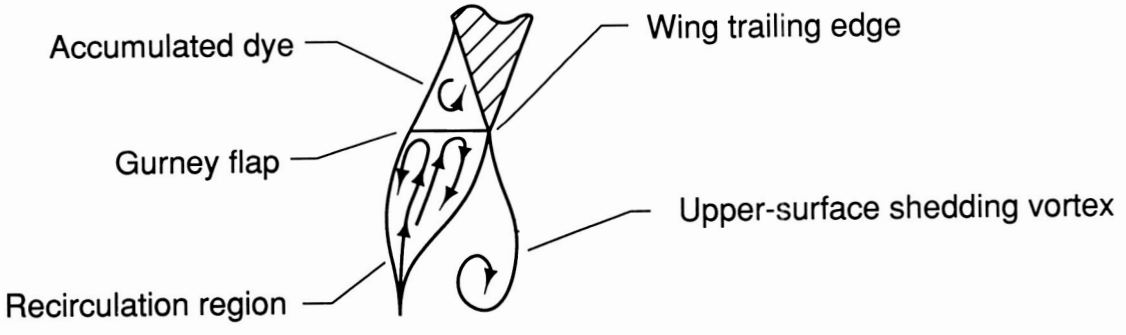

(c) Flow inside recirculation region.

Figure 18. Flow near Gurney flap.

NASA
National Aeronautics and Space Administration

Report Documentation Page

1. Report No.	2. Government Accession No.	3. Recipient's Catalog No.
NASA TM-4071		

4. Title and Subtitle	5. Report Date
A Water Tunnel Study of Gurney Flaps	November 1988
	6. Performing Organization Code
7. Author(s)	8. Performing Organization Report No.
Dan H. Neuhart and Odis C. Pendergraft, Jr.	L-16467
9. Performing Organization Name and Address	10. Work Unit No.
NASA Langley Research Center Hampton, VA 23665-5225	763-01-31-16
	11. Contract or Grant No.
12. Sponsoring Agency Name and Address	13. Type of Report and Period Covered
National Aeronautics and Space Administration Washington, DC 20546-0001	Technical Memorandum
	14. Sponsoring Agency Code

15. Supplementary Notes

Dan H. Neuhart: PRC Systems Services, a Division of Planning Research Corporation, Hampton, Virginia.

Odis C. Pendergraft, Jr.: Langley Research Center, Hampton, Virginia.

16. Abstract

Several Gurney flap configurations were tested in the Langley 16- by 24-Inch Water Tunnel. Relative to the wing without the flaps, these devices provided an increased region of attached flow on the wing upper surface. The recirculation region behind the flap was visualized and shown to be consistent with hypotheses stated in previous research. Although the test Reynolds number for this study was several orders of magnitude below those in previous investigations, the effect of the Gurney flaps is in qualitative agreement with the investigations. This is as would be expected from first-order effects for high-lift devices.

17. Key Words (Suggested by Authors(s))	18. Distribution Statement
Gurney flaps Water tunnel tests Lift enhancement Lift devices	Unclassified—Unlimited Subject Category 02

19. Security Classif.(of this report)	20. Security Classif.(of this page)	21. No. of Pages	22. Price
Unclassified	Unclassified	20	A02

For sale by the National Technical Information Service, Springfield, Virginia 22161-2171